Sum Rules for Parallel Plate Waveguides: Experimental Results and Theory

Vakili, Iman; Gustafsson, Mats; Sjöberg, Daniel; Seviour, Rebecca; Nilsson, Martin; Nordebo, Sven

2014

CODEN:LUTEDX/(TEAT-7229)/1-20/(2014)

Sum Rules for Parallel Plate Waveguides: Experimental Results and Theory

**Iman Vakili, Mats Gustafsson, Daniel Sjöberg,
Rebecca Seviour, Martin Nilsson, and Sven Nordebo**

Electromagnetic Theory
Department of Electrical and Information Technology
Lund University
Sweden

Iman Vakili, Mats Gustafsson, Daniel Sjöberg, and Martin Nilsson
{Iman.Vakili, Mats.Gustafsson, Daniel.Sjoberg, Martin.Nilsson}@eit.lth.se

Department of Electrical and Information Technology
Electromagnetic Theory
Lund University
P.O. Box 118
SE-221 00 Lund
Sweden

Rebecca Seviour
R.Seviour@hud.ac.uk

Department of Physics
Huddersfield University
Huddersfield
UK

Sven Nordebo
sven.nordebo@lnu.se

School of Computer Science
Physics and Mathematics
Linnaeus University
SE-351 95 Växjö
Sweden

Editor: Gerhard Kristensson

Abstract

An experimental approach to verify the forward scattering sum rule for periodic structures is presented. This approach allows an upper bound on the total cross section integrated over a bandwidth from a simple static problem to be found. Based on energy conservation, the optical theorem is used to construct a relation between the total cross section and the forward scattering of periodic structures as well as single scatterers inside a parallel plate waveguide. Dynamic measurements are performed using a parallel plate waveguide and a parallel plate capacitor is utilized to find the static polarizability. Convex optimization is introduced to identify the total scattering in the dynamic measurements. The results show that the all spectrum interaction between the electromagnetic field and an object are proportional to the static polarizability of the object.

1 Introduction

The scattering properties of periodic structures have been a research topic for over a century, used to study a diverse range of systems from, electron transport in nanostrutures to EM wave propagation. Although determining the dynamic properties of an object using experimental scattering techniques can be very problematic, especially when the phase of the wave has to be accurately measured. In this paper we present a relative scattering technique for EM wave propagation over an arbitrary object, which enables insight into the objects dynamic properties, without the need for difficult phase calibrations. In terms of forward scattering, the optical theorem relates the real part of the forward scattering amplitude to the total cross section of any scatterer [13, 19, 27]. The forward scattering sum rule shows that the total cross section of an object integrated over all wavelengths is proportional to the static polarizability of the object. This simple relation offers an understanding of the total interaction between the EM field and an object over the entire spectrum. This was first discussed by Purcell for dielectric spheroids [21], then generalized to arbitrary objects in [6, 25]. The sum rule has in recent years been used to introduce bounds on antennas [7–9, 24], metamaterials [26], and extraordinary transmission [10].

The optical theorem and the forward scattering sum rule have recently been generalized to 1D and 2D periodic structures in [12]. Moreover the scattered and absorbed power from an incident plane wave is known to be proportional to $\operatorname{Im} h(k)$, where $h(k) = \mathrm{i}2(1 - T(k))A$ is a Herglotz function [3, 12, 20] (or a positive real function [14]), where $\mathrm{i}^2 = -1$. Here, A is the cross sectional area of the unit cell and T is the co-polarized part of the fundamental mode transmission coefficient.

In this paper, the optical theorem and the forward scattering sum rule are extended to the case of parallel plate waveguides. The waveguide is used for wideband scattering characterization of materials. We show that this set-up can be used as a quasi-2D experimental methodology to find the scattering properties of one-dimensional periodic structures. Properties of the positive real functions, together with convex optimization [4] are utilized to combat the noise level in the system.

The low-frequency asymptotic expansion of the positive real function [11] (similar to Herglotz and Nevanlinna functions [3]) gives the relationship between the dynamic measurements and the static polarizability. In order to measure the static properties, a basic measurement set-up consisting of a parallel plate capacitor is used. The static polarizability is deduced from the small difference of the capacitance when the object is inserted in the capacitor [16].

The results show that the entire spectrum interaction between the electromagnetic field and the periodic structure in a parallel plate waveguide is proportional to the static polarizability that can be found from a parallel plate capacitor, regardless of shape and resonant behavior. This simple approach provides physical insight into the total cross section integrated over the bandwidth of any scatterer. The method is applicable for frequency selective structures [18], metamaterials [5, 23], and electromagnetic band gap structures [29].

The remainder of the paper is structured as follows. The optical theorem for periodic structures as well as single scatterer in a parallel plate waveguide are presented in Section 2. Forward scattering sum rules are discussed in Section 3. In Section 4, we report a passive system identification using convex optimization. The experimental methodology is presented in Section 5, and numerical examples are illustrated in Section 6. The paper is concluded in Section 7.

2 Optical theorem in a parallel plate waveguide

In this section the optical theorem for a parallel plate waveguide is presented. As shown in Fig. 1ab, the optical theorem is calculated for a one-dimensional periodic structure in Section 2.1, and for finite objects inside an imaginary cylinder in Section 2.2, see Fig. 1c.

2.1 Periodic structures

We consider a one-dimensional planar periodic structure inserted inside a parallel plate waveguide. The structure has infinite periodicity in the y-direction and is oriented in the yz-plane (see Fig. 1ab). A linearly polarized time harmonic TEM mode, $\boldsymbol{E}_{\mathrm{i}}(\boldsymbol{r}) = \hat{\boldsymbol{z}} E_0 \mathrm{e}^{-\mathrm{j}kx}$, impinges upon the periodic structure at normal incidence, where k denotes the wavenumber and the time convention $\mathrm{e}^{\mathrm{j}\omega t}$ is used. The transmitted and the reflected fields are denoted $\boldsymbol{E}_{\mathrm{t}}$ and $\boldsymbol{E}_{\mathrm{r}}$, respectively.

The transverse components of the transmitted field, denoted by $\boldsymbol{E}_{\mathrm{t}}^{\mathrm{yz}}$ below, are expanded in a combination of waveguide and Floquet modes (the normal components can be derived from the transverse components and do not provide additional degrees of freedom). The spectral decomposition of the modes, taking the periodicity in y-direction and the electric boundary conditions in z-direction into account can be written as

$$\boldsymbol{E}_{\mathrm{t}}^{\mathrm{yz}}(k;\boldsymbol{r}) = \sum_{m=-\infty}^{\infty} \sum_{n=0}^{\infty} \sum_{\nu=\mathrm{TE,TM}} E_{mn\nu}(k) \boldsymbol{E}_{tn\nu}^{\mathrm{yz}}(z) \mathrm{e}^{-\mathrm{j}(k_x x + m2\pi y/a)}, \tag{2.1}$$

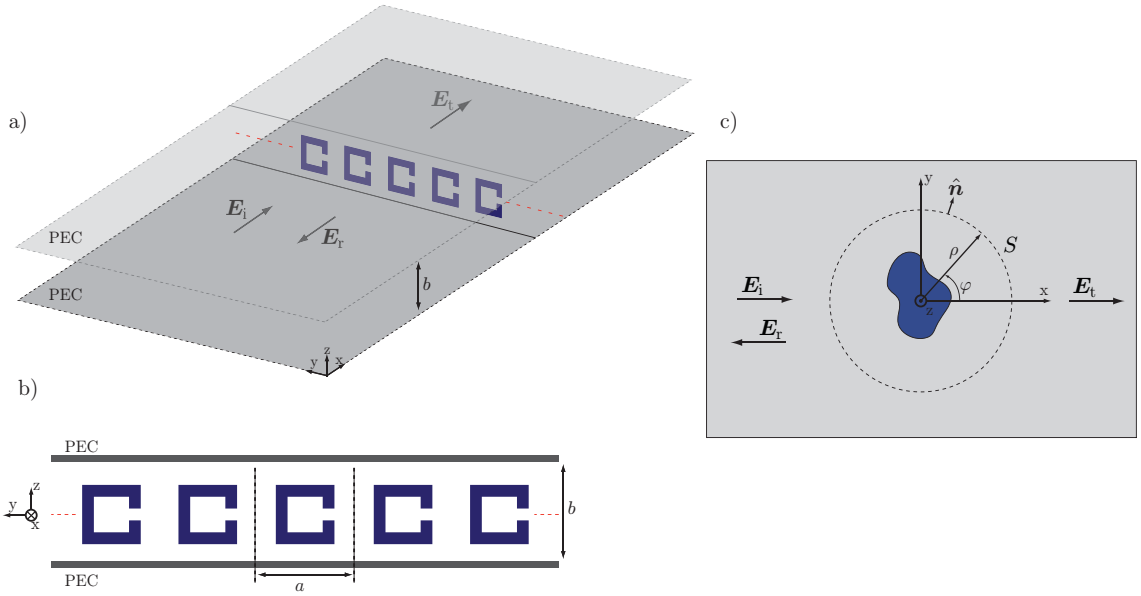

Figure 1: Scattering geometry for periodic objects inside the parallel plate waveguide. a) perspective view. $\boldsymbol{E}_\mathrm{i}$ is the incident field, $\boldsymbol{E}_\mathrm{t}$ the transmitted field, and $\boldsymbol{E}_\mathrm{r}$ denotes the reflected field. b) front view. The unit cell size is $a \times b$. c) top view of the parallel plate waveguide. The imaginary surface S is a cylinder of radius ρ and normal vector $\hat{\boldsymbol{n}}$, that encloses the object.

where $k_x = \sqrt{k^2 - (m2\pi/a)^2 - (n\pi/b)^2}$, a is the length of the unit cell in the y-direction and b is the height of the waveguide, see Fig. 1b. Note the extra factor of 2 in the term $m2\pi/a$ compared to $n\pi/b$. When m is large enough, the corresponding modes are evanescent. Here, $\boldsymbol{E}^{\mathrm{yz}}_{tn\nu}$ denotes the transverse components of the vector basis functions for waveguide modes, which are $\boldsymbol{E}^{\mathrm{yz}}_{tn\nu} = \sqrt{\epsilon_n}\cos(\frac{n\pi z}{b})\hat{\boldsymbol{z}}$ for $\nu = \mathrm{TM}$ (where $\epsilon_n = 1$ for $n = 0$ and $\epsilon_n = 2$ for $n \neq 0$), and $\boldsymbol{E}^{\mathrm{yz}}_{tn\nu} = \sqrt{2}\sin(\frac{n\pi z}{b})\hat{\boldsymbol{y}}$ for $\nu = \mathrm{TE}$ and $n > 0$, see [17, p. 64] for more details. The expansion coefficients behind the structure are,

$$E_{mn\nu} = \frac{1}{ab}\int_0^b\int_0^a \boldsymbol{E}^{\mathrm{yz}}_{\mathrm{t}}(k;0,y,z)\cdot\boldsymbol{E}^{\mathrm{yz}*}_{tn\nu}(z)\mathrm{e}^{\mathrm{j}m2\pi y/a}\,\mathrm{d}y\,\mathrm{d}z, \tag{2.2}$$

where, $(*)$ denotes the complex conjugate. A general incident field can be expanded in the corresponding modes, which are related to the modes of the transmitted field by a linear mapping quantified by the transmission coefficient $T_{mn\nu,m'n'\nu'}$. In our case, we consider an incident field consisting of only the TEM mode ($m' = 0$, $n' = 0$, and $\nu' = \mathrm{TM}$), and study the corresponding transmitted mode ($m = 0$, $n = 0$, and $\nu = \mathrm{TM}$) and define the co-polarized transmission coefficient as $T = T_{00\mathrm{TM},00\mathrm{TM}}$.

The optical theorem for periodic structures is based on energy conservation and relates the forward scattered field to the total cross section [12]. The incident power per unit cell is denoted by P_i. The transmitted power is $P_\mathrm{t} = |T|^2 P_\mathrm{i} + P_{\mathrm{t}1}$.

Here, $|T|^2 P_\mathrm{i}$ is the co-polarized transmitted power in the TEM mode and P_t1 is the transmitted power for the remaining modes. The difference between the incident and the sum of the reflected and transmitted power is the absorbed power, $P_\mathrm{a} = P_\mathrm{i} - P_\mathrm{r} - |T|^2 P_\mathrm{i} - P_\mathrm{t1}$, and the sum of the reflected power and the power in the scattered part of the transmitted field is the scattered power, $P_\mathrm{s} = P_\mathrm{r} + |1-T|^2 P_\mathrm{i} + P_\mathrm{t1}$. The total power is the sum of the absorbed and scattered power and can be expressed as

$$P_\mathrm{tot} = P_\mathrm{a} + P_\mathrm{s} = 2\,\mathrm{Re}\{1 - T(k)\} P_\mathrm{i}. \tag{2.3}$$

By considering the incident power per unit cell, $P_\mathrm{i} = A|E_0|^2/(2\eta_0)$ and normalizing both sides of (2.3) by the incident power flux, $|E_0|^2/2\eta_0$, the total (extinction) cross section becomes

$$\sigma_\mathrm{tot} = \sigma_\mathrm{a} + \sigma_\mathrm{s} = 2\,\mathrm{Re}\{1 - T\} A, \tag{2.4}$$

where $A = ab$. This relation between the total cross section and the transmission coefficient is the optical theorem for periodic objects in a parallel plate waveguide.

2.2 Bounded scatterer

In this subsection, the optical theorem is investigated for a non-periodic structure bounded by an imaginary cylinder. Assume an incident wave propagating in the positive x-direction, linearly polarized in the z-direction $\boldsymbol{E}_\mathrm{i} = \hat{\boldsymbol{z}} E_0 \mathrm{e}^{-\mathrm{j}kx}$. A scatterer of arbitrary shape and material placed inside the parallel plate waveguide. Following [13, p. 501], the sum of the absorbed and scattered power, here denoted the total power is

$$\begin{aligned} P_\mathrm{tot} = P_\mathrm{a} + P_\mathrm{s} &= \frac{1}{2}\,\mathrm{Re} \int_S \hat{\boldsymbol{n}} \cdot [-(\boldsymbol{E}_\mathrm{i} + \boldsymbol{E}_\mathrm{s}) \times (\boldsymbol{H}_\mathrm{i} + \boldsymbol{H}_\mathrm{s})^* + \boldsymbol{E}_\mathrm{s} \times \boldsymbol{H}_\mathrm{s}^*]\,\mathrm{dS} \\ &= -\frac{1}{2}\,\mathrm{Re} \int_S \hat{\boldsymbol{n}} \cdot (\boldsymbol{E}_\mathrm{s} \times \boldsymbol{H}_\mathrm{i}^* + \boldsymbol{E}_\mathrm{i} \times \boldsymbol{H}_\mathrm{s}^*)\,\mathrm{dS}, \end{aligned} \tag{2.5}$$

where the surface S encloses the scatterer and $\hat{\boldsymbol{n}} = \hat{\boldsymbol{\rho}} = \hat{\boldsymbol{x}} \sin\phi + \hat{\boldsymbol{y}} \cos\phi$ is the outward pointing normal vector (see Fig. 1c). The subscript s stands for the scattered fields that represent the difference between the fields in the presence and absence of the object, *i.e.*, $\boldsymbol{E}_\mathrm{s} = \boldsymbol{E} - \boldsymbol{E}_\mathrm{i}$. The surface S does not include the metal boundaries at $z = 0$ and $z = b$, since the power flux is zero through these boundaries. Using the real part to shift the last complex conjugate from $\boldsymbol{H}_\mathrm{s}^*$ to $\boldsymbol{E}_\mathrm{i}$, $\hat{\boldsymbol{y}} = \hat{\boldsymbol{z}} \times \hat{\boldsymbol{x}}$, and inserting the expression for the incident field, we get

$$P_{\text{tot}} = -\frac{1}{2}\,\text{Re}\int\limits_S E_0^* \text{e}^{\text{j}kx}\hat{\boldsymbol{n}}\cdot(-\boldsymbol{E}_\text{s}\times\hat{\boldsymbol{y}}\eta_0^{-1}+\hat{\boldsymbol{z}}\times\boldsymbol{H}_\text{s})\,\text{dS}$$

$$= \frac{-1}{2\eta_0}\,\text{Re}\int\limits_0^b\int\limits_0^{2\pi} E_0^*\text{e}^{\text{j}kx}\hat{\boldsymbol{z}}\cdot(\boldsymbol{E}_\text{s}(\hat{\boldsymbol{n}}\cdot\hat{\boldsymbol{x}})+\eta_0\boldsymbol{H}_\text{s}\times\hat{\boldsymbol{n}})\,\text{d}\phi\,\text{d}z$$

$$= \frac{-b}{2\eta_0}\,\text{Re}\int\limits_0^{2\pi} E_0^*\text{e}^{\text{j}kx}\hat{\boldsymbol{z}}\cdot\langle\boldsymbol{E}_\text{s}(\hat{\boldsymbol{n}}\cdot\hat{\boldsymbol{x}})+\eta_0\boldsymbol{H}_\text{s}\times\hat{\boldsymbol{n}}\rangle\,\text{d}\phi, \quad (2.6)$$

where $\langle . \rangle$ denotes the mean value of the fields over the height of the waveguide. The scattered field can be expanded in cylindrical modes, see Appendix A. There, it is shown that the mean value in (2.6) is nonzero only for the zeroth order mode, which is co-polarized to the incident plane wave. By normalizing the total power with the incident power flux, $|E_0|^2/2\eta_0$, the total cross section becomes

$$\sigma_{\text{tot}} = -\,\text{Re}\Big\{\frac{b}{|E_0|}\int\limits_0^{2\pi}\text{e}^{\text{j}kx}\hat{\boldsymbol{z}}\cdot\langle\boldsymbol{E}_\text{s}(\hat{\boldsymbol{n}}\cdot\hat{\boldsymbol{x}})+\eta_0\boldsymbol{H}_\text{s}\times\hat{\boldsymbol{n}}\rangle\,\text{d}\phi\Big\}, \quad (2.7)$$

where the integral in (2.7) is similar to the far-field amplitude, f_s, in two dimensions which is given by [28]

$$f_\text{s}(k) = \frac{\text{j}k}{4}\int\limits_0^{2\pi}\text{e}^{\text{j}kx}\hat{\boldsymbol{z}}\cdot\langle\boldsymbol{E}_\text{s}(\hat{\boldsymbol{n}}\cdot\hat{\boldsymbol{x}})+\eta_0\boldsymbol{H}_\text{s}\times\hat{\boldsymbol{n}}\rangle\,\text{d}\phi, \quad (2.8)$$

where the co-polarized two-dimensional scattered far field $\boldsymbol{E}_\text{s}\sim\hat{\boldsymbol{z}}f_\text{s}\sqrt{\frac{2}{\pi\text{j}k\rho}}\text{e}^{-\text{j}k\rho}$ and therefore, the total cross section can be written as

$$\sigma_{\text{tot}} = -4b\,\text{Re}\left\{\frac{E_0^* f_\text{s}(k)}{\text{j}k|E_0|^2}\right\}. \quad (2.9)$$

The normalization by the height of the waveguide gives the two-dimensional total cross section.

3 Forward scattering sum rules

The forward scattering sum rule is used to find an upper bound on the total cross section of any scatterer. The identities stating that the sum or integral of a variable has a certain value are categorized as sum rules and are mostly derived using holomorphic functions such as positive real or Herglotz (Nevanlinna) functions [3, 11, 14, 20]. In this paper the positive real (PR) function, $\mathscr{P}(\kappa)$, is given by the forward scattering amplitude derived in (2.4) and (2.9), where $\kappa = \zeta + \text{j}k$. In both cases the PR

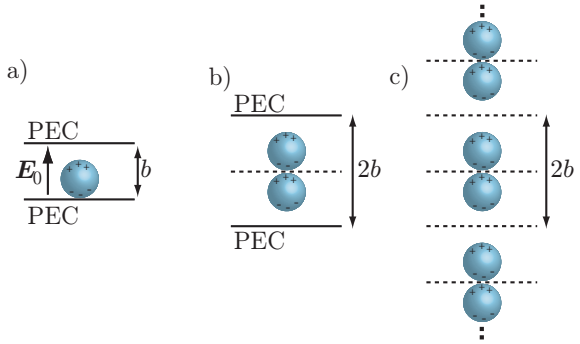

Figure 2: Periodic equivalence problem. a) An object is placed in an arbitrary position between the plates of a capacitor. b) An equivalent problem for part-a by placing the object and its image at the mid point between two plates. c) The equivalent periodic problem.

function is holomorphic and $\mathrm{Re}\{\mathscr{P}(\kappa)\} \geq 0$ for $\mathrm{Re}\{\kappa\} > 0$ [12] and is given by

$$\mathscr{P}(\kappa) = \begin{cases} 2(1-T(\kappa))A & \text{for a periodic structure} \\ -\frac{4b}{\kappa|E_0|^2} E_0^* f_{\mathrm{s}}(\kappa) & \text{for a single scatterer} \end{cases} \tag{3.1}$$

where the total cross section $\sigma_{\mathrm{tot}} = \mathrm{Re}\{\mathscr{P}(\kappa)\}$.

The low-frequency asymptotic expansion is obtained from Maxwell equations by an expansion in the fields [22], giving

$$\mathscr{P}(\kappa) = \kappa\big(\hat{\boldsymbol{e}} \cdot \boldsymbol{\gamma}_{\mathrm{e}} \cdot \hat{\boldsymbol{e}} + (\hat{\boldsymbol{k}} \times \hat{\boldsymbol{e}}) \cdot \boldsymbol{\gamma}_{\mathrm{m}} \cdot (\hat{\boldsymbol{k}} \times \hat{\boldsymbol{e}})\big) + o(\kappa) \tag{3.2}$$

as $\kappa \hat{\to} 0$, where $\hat{\to}$ is the limit inside the right half plane and $|\arg(\kappa)| < \frac{\pi}{2} - \delta$ for a small positive δ, and $\boldsymbol{\gamma}_{\mathrm{e}}$ and $\boldsymbol{\gamma}_{\mathrm{m}}$ are the electric and magnetic static polarizability dyadics, respectively. This equation gives the slope of the forward scattering at low frequencies and as it is shown in Section 6, for long wavelengths compared to the size of the object this gives a good approximation of the static polarizability. The parallel plate waveguide in the static limit, $k \to 0$, is equivalent to a parallel plate capacitor with a uniform field distribution, $\boldsymbol{E}_0$, as shown in Fig. 2a. Here, $\boldsymbol{\gamma}_{\mathrm{e}}$ and $\boldsymbol{\gamma}_{\mathrm{m}}$ are identified as the polarizabilities of an object in the presence of the metal plates (in the periodic case this is understood as the polarizability per unit cell). This can be computed directly using proper boundary conditions in the finite element method, or the corresponding Green's function in the method of moments. The methods for periodic structures in [12, 22] can also be used, since $\boldsymbol{\gamma}_{\mathrm{e}}$ equals half the polarizability of a mirror-symmetric, periodic structure with unit cell of length $2b$, as seen in Fig. 2bc.

The sum rule relates the total cross section over all wavelengths to the static polarizability and is given by [3]

$$\frac{2}{\pi} \int_0^\infty \frac{\sigma_{\mathrm{tot}}(k; \hat{\boldsymbol{k}}, \hat{\boldsymbol{e}})}{k^2} \, \mathrm{d}k = \hat{\boldsymbol{e}} \cdot \boldsymbol{\gamma}_{\mathrm{e}} \cdot \hat{\boldsymbol{e}} + (\hat{\boldsymbol{k}} \times \hat{\boldsymbol{e}}) \cdot \boldsymbol{\gamma}_{\mathrm{m}} \cdot (\hat{\boldsymbol{k}} \times \hat{\boldsymbol{e}}), \tag{3.3}$$

where $\hat{\boldsymbol{e}}$ is the real valued unit vector along the polarization of the incident field. The integration on the left hand side determines the dynamic behavior of the scatterer and the right hand side can be found from the static properties. The sum rule is used to derive an upper bound on the total cross section integrated over a bandwidth [3].

In this paper we use a parallel plate waveguide to determine the integral value on the left hand side and a parallel plate capacitor to measure the static polarizability on the right hand side of (3.3). The sum rule is valid for passive structures that do not support currents in the low frequency limit, *i.e.*, that do not short circuit the plates.

4 Passive system identification using convex optimization

Convex optimization [4] together with the properties of positive real functions are used to identify the measured passive system. A symmetric PR function can be represented as

$$\mathscr{P}(\kappa) = b_1\kappa + \int_{-\infty}^{\infty} \frac{\kappa}{\xi^2+\kappa^2}\,\mathrm{d}G(\xi), \tag{4.1}$$

for $\operatorname{Re}\kappa > 0$, where b_1 is a real valued and non-negative constant, $\kappa = \zeta + \mathrm{j}k$ is the Laplace parameter, and $G(\xi)$ is a positive and finite measure such that $\int_{\mathbb{R}} \mathrm{d}G(\xi)/(1+\xi^2) < \infty$. The spectral function $G(\xi)$ is uniquely defined as [14]

$$G(\xi) = \frac{1}{\pi}\lim_{\zeta\to 0^+}\int_0^{\xi} \operatorname{Re}\mathscr{P}(\zeta+\mathrm{j}k)\,\mathrm{d}k. \tag{4.2}$$

Using the low/high-frequency asymptotic expansions of $\mathscr{P}(\kappa)$ based on the representation (4.1) in the limit $\zeta \to 0^+$, and considering the even measure of $G(-\xi) = G(\xi)$, we can write the first integral identity as [11]

$$\frac{2}{\pi}\int_0^{\infty} \frac{\operatorname{Re}\mathscr{P}(\mathrm{j}k)}{k^2}\,\mathrm{d}k = a_1 - b_1, \tag{4.3}$$

where the low frequency asymptotic of $\mathscr{P}$ is $a_1\kappa + o(\kappa)$ and the high frequency asymptotic is $b_1\kappa + o(\kappa)$. Here, a_1 and b_1 are real valued and non-negative constants. Assuming that the positive real function $\mathscr{P}$ is sufficiently regular on the frequency axis $\kappa = \mathrm{j}k$, its imaginary part is given by

$$\operatorname{Im}\mathscr{P}(\mathrm{j}k) = b_1 k + \frac{1}{\pi}\int_{-\infty}^{\infty} \frac{k}{\xi^2-k^2}\operatorname{Re}\mathscr{P}(\mathrm{j}\xi)\,\mathrm{d}\xi = b_1 k + \frac{1}{\pi}\int_{-\infty}^{\infty} \frac{1}{\xi-k}\operatorname{Re}\mathscr{P}(\mathrm{j}\xi)\,\mathrm{d}\xi, \tag{4.4}$$

where the integral is identified as the Hilbert transform. The second equality is known as the Plemelj formula [20], it should be noted that the imaginary part of

$\mathscr{P}$ is odd symmetric with $\operatorname{Im}\mathscr{P}(-\mathrm{j}k) = -\operatorname{Im}\mathscr{P}(\mathrm{j}k)$. The linear transform in (4.4) acts as a linear operator on the real response $\operatorname{Re}\mathscr{P}(\mathrm{j}k)$ to yield the imaginary part $\operatorname{Im}\mathscr{P}(\mathrm{j}k)$ of the passive system. This can be treated as a convex optimization problem with constraints on the unknown quantities $b_1 \geq 0$ and $\operatorname{Re}\mathscr{P}(\mathrm{j}k) \geq 0$. As a finite-dimensional approximation, the positive and symmetric measure $\operatorname{Re}\mathscr{P}(\mathrm{j}k)$ is modeled here by

$$\operatorname{Re}\mathscr{P}(\mathrm{j}k) = \sum_{n=0}^{N-1} x_n[p(k-(n+n_0)\Delta k) + p(k+(n+n_0)\Delta k)], \tag{4.5}$$

where x_n is a non-negative real valued variable, Δk is the frequency step, n_0 is an offset parameter and $p(k)$ is a triangular pulse-shape ($p(k) = 1-|k|/\Delta k$ for $|k| \leq \Delta k$ and 0 otherwise). By inserting the approximated $\operatorname{Re}\mathscr{P}(\mathrm{j}k)$ in (4.4) the imaginary part becomes

$$\operatorname{Im}\mathscr{P}(\mathrm{j}k) = b_1 k + \sum_{n=0}^{N-1} x_n[\tilde{p}(k-(n+n_0)\Delta k) + \tilde{p}(k+(n+n_0)\Delta k)], \tag{4.6}$$

where $\tilde{p}(k)$ is the Hilbert transform of the pulse shape $p(k)$ given by

$$\begin{aligned}\tilde{p}(k) &= \frac{1}{\pi}\int_{-\infty}^{\infty} \frac{1}{\xi - k} p(\xi)\,\mathrm{d}\xi \\ &= \frac{2k\ln|k| - (k-\Delta k)\ln|k-\Delta k| - (k+\Delta k)\ln|k+\Delta k|}{\pi\Delta k}\end{aligned} \tag{4.7}$$

with $\tilde{p}(\pm\Delta k) = \mp(2\ln 2)/\pi$ and $\tilde{p}(0) = 0$. By applying the finite-dimensional approximation the sum rule in (4.3) can be represented as

$$\frac{1}{\pi\Delta k}\sum_{n=0}^{N-1} x_n \ln\frac{(n+n_0)^2}{(n+n_0-1)(n+n_0+1)} = a_1 - b_1. \tag{4.8}$$

Considering the real and imaginary responses of $\mathscr{P}$, and also the sum rule in (3.3), we define the convex optimization problem

$$\begin{aligned} \text{minimize} \quad & \left\| \mathscr{P}(\mathrm{j}k) - \mathscr{P}^{(\mathrm{M})}(\mathrm{j}k) \right\| \\ \text{subject to} \quad & \operatorname{Re}\mathscr{P}(\mathrm{j}k) \geq 0,\ k \in [k_0, k_3], \\ & \frac{2}{\pi}\int_{k_0}^{k_3} \frac{\operatorname{Re}\mathscr{P}(\mathrm{j}k)}{k^2}\,\mathrm{d}k \leq \gamma_u, \end{aligned} \tag{4.9}$$

where $\mathscr{P}^{(\mathrm{M})}(\mathrm{j}k)$ is the measured forward scattering for $k \in [k_1, k_2]$ which is inside the modeling interval $k_0 < k_1 < k_2 < k_3$ and γ_u is an upper bound on the sum rule. The norm is defined as

$$\left\| \mathscr{P}(\mathrm{j}k) - \mathscr{P}^{(\mathrm{M})}(\mathrm{j}k) \right\|^2 = \int_{k_1}^{k_2} w(k) |\mathscr{P}(\mathrm{j}k) - \mathscr{P}^{(\mathrm{M})}(\mathrm{j}k)|^2\,\mathrm{d}k, \tag{4.10}$$

where $w(k)$ is a positive weighting function.

Consider the measurement model as $\mathscr{P}(\mathrm{j}k) = f(k) + g(k)n(k)$, where $f(k)$ and $g(k)$ are given, and $n(k)$ is uncorrelated complex Gaussian noise with variance σ_n^2. Hence, the variance of the uncorrelated measurement noise is $|g(k)|^2\sigma_n^2$ and the proper weighting function in a Maximum Likelihood estimation [15] is $w(k) = |g(k)|^{-2}$, and particularly, in the methodology of this paper we find that

$$w(k) = |g(k)|^{-2} = \frac{k|S_{21,\mathrm{emp}}|^2}{4\pi d}, \tag{4.11}$$

where $S_{21,\mathrm{emp}}$ is the scattering parameter for the empty setup (see Section 5.1 for more details).

5 Experimental Methodology

The methodology used to illustrate the sum rule is presented in this section. A parallel plate waveguide is used to investigate the dynamic properties, and a parallel plate capacitor is used to determine the static properties of an object.

5.1 Parallel plate waveguide

A parallel plate waveguide is used to test the scattering properties of different objects. Two in-house fabricated wide-band TEM horn antennas are placed inside the waveguide and are fed via the lower plate as shown in Fig. 3a. The antennas are separated by a distance of 0.98 m and the object is placed in the middle of the waveguide. The TEM horn antennas are supported by a piece of Rohacell material with relative permittivity, $\epsilon_\mathrm{r} \approx 1$. Microwave flat absorbers are placed around the waveguide to reduce the internal reflections and external interferences. The separation between two plates is 21.3 mm, which gives the first higher order mode at $f \approx 7\,\mathrm{GHz}$.

In order to measure the forward scattering, the scattered field, $\boldsymbol{E}_\mathrm{s}$, is determined from the difference between the fields in the presence and the absence of the object. We consider a plane wave incidence, $\boldsymbol{E}_\mathrm{i}(\boldsymbol{r}) = \boldsymbol{E}_0\mathrm{e}^{-\mathrm{j}k_\mathrm{x}x}$, to an object confined between the plates. The co-polarized scattered field in the far-field region can be expressed as

$$\hat{\boldsymbol{z}} \cdot \boldsymbol{E}_\mathrm{s} \sim f_\mathrm{s}\sqrt{\frac{2}{\pi\mathrm{j}k\rho}}\mathrm{e}^{-\mathrm{j}k\rho}. \tag{5.1}$$

The distance between two antennas is denoted by d and the separation between the object and the transmitting antenna is d_1. The scattered field received by the antenna in the absence of the object is

$$E_{r,0} = f_0\sqrt{\frac{2}{\pi\mathrm{j}kd}}\mathrm{e}^{-\mathrm{j}kd}, \tag{5.2}$$

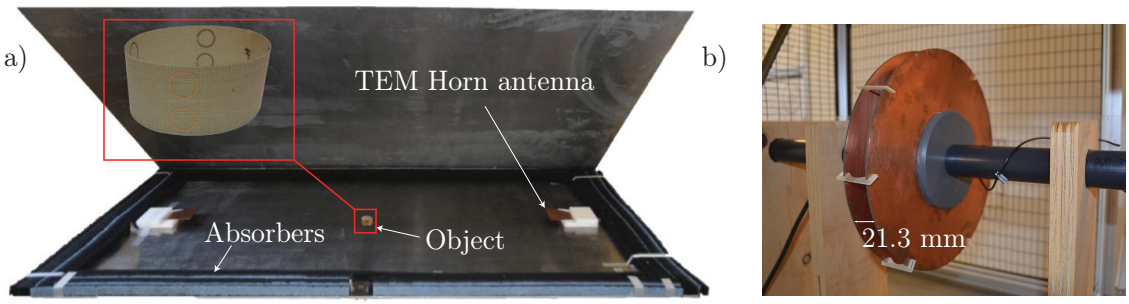

Figure 3: a) The parallel plate waveguide setup consists of two TEM horn antennas and microwave flat absorbers. The distance between the antennas is 98 cm and the object is placed at the midpoint between the antennas. The two plates are $150 \times 100\,\mathrm{cm}^2$ and separated by 21.3 mm. b) The parallel plate capacitor setup consists of two circular copper plates held by plastic arms. The distance between the plates is 21.3 mm and is fixed by plastic distance supports

where f_0 is the far-field amplitude generated by the transmitting antenna. The object is assumed to be in the far-field of the antenna and thus the far-field amplitude at the object is also f_0.

The incident field on the object is given by

$$E_0 = f_0 \sqrt{\frac{2}{\pi \mathrm{j} k d_1}} \mathrm{e}^{-\mathrm{j}kd_1}. \tag{5.3}$$

This electric field induces currents on the object and it acts as a scatterer. The resulting electric field on the receiving antenna in the presence of the object is denoted by $E_{\mathrm{r,s}}$ and thus the scattered field of the object itself can be written as $E_{\mathrm{s}} = E_{\mathrm{r,s}} - E_{\mathrm{r},0}$. According to (2.9), the positive real function is defined as

$$\mathscr{P}_b(\mathrm{j}k) = \frac{-4 f_{\mathrm{s}}}{\mathrm{j}k E_0} = \frac{4}{\mathrm{j}k} \left(1 - \frac{E_{r,s}}{E_{r,0}}\right) \sqrt{\frac{\pi \mathrm{j} k d_1 (d - d_1)}{2d}}, \tag{5.4}$$

where $\mathscr{P}_b$ denotes the PR defined in (3.1) normalized with the height of the waveguide, *i.e.*, $\mathscr{P}_b = \mathscr{P}/b$, and this can be approximated by:

$$\mathscr{P}_b(\mathrm{j}k) = \frac{-4 f_{\mathrm{s}}}{\mathrm{j}k E_0} = \frac{4}{\mathrm{j}k} \left(1 - \frac{S_{21,\mathrm{obj}}}{S_{21,\mathrm{emp}}}\right) \sqrt{\frac{\pi \mathrm{j} k d_1 (d - d_1)}{2d}}, \tag{5.5}$$

where $S_{21,\mathrm{obj}}$ is the ratio between the out-coming wave at the port of the receiving antenna and the incident wave at the port of the transmitting antenna in the presence of the object. For the periodic structures discussed in 2.1, we use the top equation in (3.1) to find the forward scattering, $\mathscr{P}$, where the transmission coefficient is defined as $T = S_{21,\mathrm{obj}}/S_{21,\mathrm{emp}}$.

5.2 Parallel plate capacitor

The parallel plate capacitor consists of two circular shaped copper sheets printed on a dielectric substrate made of FR4 substrate with relative dielectric constant, $\epsilon_{\rm r} \approx 4.4$, and is used to determine the polarizability (see Fig. 3b). A Faraday cage, and a ground plane, are used to mitigate interference and current flows between different grounds in the system. An Agilent 4294A Precision Impedance Analyzer is used to measure the capacitance at $f = 1\,\text{MHz}$.

The relation between the capacitance change and the polarizability of a bounded object inside the parallel plate capacitor is given by [16]

$$\gamma_{\rm e} = \hat{\boldsymbol{z}} \cdot \boldsymbol{\gamma}_{\rm e} \cdot \hat{\boldsymbol{z}} = \frac{\Delta C d^2}{\epsilon_0}, \tag{5.6}$$

where $\Delta C = C_0 - C_{\rm e}$ is the difference between the capacitance in presence, C_0, and the absence, $C_{\rm e}$, of the object, d is the separation between the two plates and ϵ_0 is the vacuum permittivity. For each sample the measurement was repeated 10 times to mitigate the possible positioning or distance errors. As seen in Fig. 3b, six plastic distance precisions are placed on the edges of the plates to keep the distance constant in different measurements. The separation distance, $d = 21.3\,\text{mm}$, is the same as the height of the parallel plate waveguide and the objects (more details in Section 6).

6 Experimental results

In this section, four different scattering objects are considered to illustrate the forward scattering sum rule. In each case, the dynamic measurement in the parallel plate waveguide is shown. Then convex optimization is applied to predict the low frequency limits and is followed by the static measurement of the object inside the parallel plate capacitor. The static polarizability is determined by the variations of the capacitance between the absence and the presence of the object placed in the middle of the plates. The static results are then compared to the total cross section computed from the dynamic measurements in the parallel plate waveguide.

6.1 Cylindrical SRR

A cylinder of split ring resonators (SRR) composed of 16 SRRs etched in $18\,\mu$m copper and supported by a $21 \times 160\,\text{mm}^2$ and $127\,\mu$m thick Arlon Diclad880 with relative permittivity, $\epsilon_{\rm r} = 2.17$, is used. The C-shaped unit element has the outer diameter $\ell = 8\,\text{mm}$, the strip width $t = 0.5\,\text{mm}$, and the gap distance $g = 0.7\,\text{mm}$. The unit element is designed to be resonant at $5.5\,\text{GHz}$.

The forward scattering of this object is measured inside the parallel plate waveguide over the frequency range $[2 - 20]\,\text{GHz}$. The resulting forward scattering, $\mathscr{P}$, is illustrated in Fig. 4a. Solid lines show the measured values averaged over 10 measurements to reduce the noise level, whereas the error level is shown with bars.

Averaging has the advantage of removing the unwanted measurement errors especially at low frequencies, which have the highest impact on determining the low frequency limit on the right hand side of the sum rule (3.3). Except for the frequencies below 3 GHz, the set-up is considered to be stable over different measurements and as seen from Fig. 4a the experimental errors are small, hence for clarity we do not show the bars in figures 4b−6a.

Convex optimization is used to compute an all-spectrum representation of the measured values according to Section 4. The dashed curves in Fig. 4b show the real and the imaginary part of the forward scattering predicted by the convex optimization problem. Since the imaginary part approaches $f = 0\,\mathrm{Hz}$ linearly, it can be used to estimate the low frequency limit in (3.3) accurately. Using the optimization solution, the value of the linear slope of the curve is estimated to $\mathscr{P}(\mathrm{j}k)/\mathrm{j}k = 3.4\,\mathrm{cm}^3$ as $k \to 0$ and the value of the integral (3.3) from 0 to 20 GHz is $2.87\,\mathrm{cm}^3$ which gives 88% of the integral over all wavelengths. It should be noted that the upper bound, γ_u, in (4.9) has been chosen using a search over an assumed range of polarizabilities in order to make sure that the corresponding constraint is active.

The solid lines in Fig. 4b represent the measured values. By integrating the total cross section, $\sigma_\mathrm{tot} = \mathrm{Re}\,\mathscr{P}$, over the frequency range of the measurement, we get $2.75\,\mathrm{cm}^3$ which is less than the value obtained from the convex optimization problem. The reason is that, first, the optimization has the advantage of neglecting negative parts due to the fact that σ_tot cannot be less than zero, and second, the integration in the optimization formulation starts from $f = 0\,\mathrm{Hz}$ according to (3.3), whereas in measurements, it starts from $f = 2\,\mathrm{GHz}$.

The parallel plate capacitor is used to measure the static polarizability of the object. The resulting value averaged over 10 measurements with standard deviation, $\sigma = 0.04\,\mathrm{cm}^3$, is estimated to $\gamma_e = 3.65\,\mathrm{cm}^3$. This is in a good agreement with low frequency limit, $\mathscr{P}(\mathrm{j}k)/\mathrm{j}k = 3.4\,\mathrm{cm}^3$ as $k \to 0$, from the dynamic measurement inside the parallel plate waveguide. Since the measured capacitances in the capacitor are in the order of picofarads, the difference can stem from small errors in the measurement set-up.

A cuboid-shaped $21 \times 120\,\mathrm{mm}^2$ Arlon Diclad 880 is used to support 8 SRRs having the same dimensions as in the previous example. The forward scattering measurement of this object is shown as solid curves in Fig. 5a. As can be seen, this structure has a stronger resonance compared to cylindrical ones, which is due to the angle of incidence and mutual coupling between elements. In spite of this, the size of the object is smaller which leads to a narrower bandwidth and a lower integral value in (3.3). The integration of the measured value from 2 to 20 GHz gives $3.10\,\mathrm{cm}^3$ and the optimal solution from 0 to 20 GHz gives $3.07\,\mathrm{cm}^3$, which is essentially the same and it shows the good agreement between the measured values and the convex optimization problem. The optimal solution gives $\mathscr{P}(\mathrm{j}k)/\mathrm{j}k = 3.57\,\mathrm{cm}^3$ as $k \to 0$ while the achieved polarizability from the capacitor is estimated to $\gamma_e = 3.53\,\mathrm{cm}^3$.

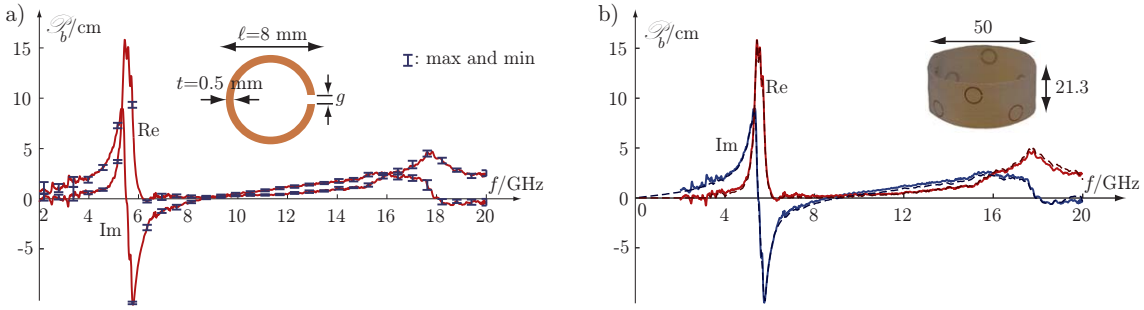

Figure 4: a)Average of the 10 measurements (solid curves) for the forward scattering for an array of circular split rings, see Fig. 4b. Maximum and minimum values over the 10 measurements are illustrated by the bars. b) Measured values (solid curves) and the optimal solution (dashed curves) for the forward scattering of a cylinder of split ring resonator with the diameter of unit element, $\ell = 8\,\mathrm{mm}$.

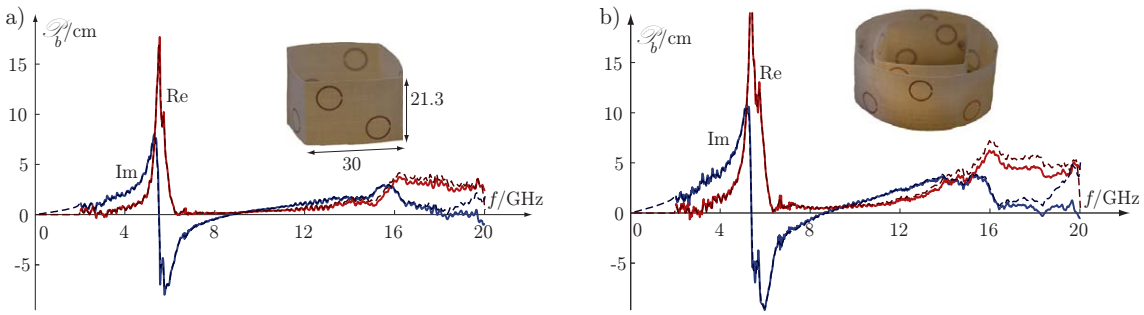

Figure 5: a) Measured values (solid curves) and the optimal solution (dashed curves) for the forward scattering of a) a cube of SRRs with the diameter of the unit element, $\ell = 8\,\mathrm{mm}$ and b) a cuboid-shaped SRR structure inside a cylinder of split ring resonators with the diameter of unit element, $\ell = 8\,\mathrm{mm}$.

6.2 Cylindrical and Cubic SRRs

Consider an object composed of a cylindrical- and a cuboid-shaped structure of SRRs (see Fig. 5b). As can be seen, the object is the combination of two structures in the Example A. The resonance frequency of this object is the same as the Example A. However, the coupling between split ring resonators causes a wider bandwidth and stronger scattering at higher frequencies. The lower left part of Fig. 5b illustrates a steeper slope of the $\mathrm{Im}\,\mathscr{P}(\mathrm{j}k)$ compared to that in Fig. 4b and Fig. 5a.

The convex optimization estimates the low frequency asymptotic to $6.51\,\mathrm{cm}^3$ as $k \to 0$ and the left hand side of the sum rule (3.3) integrated from 0 to 20 GHz to $5.58\,\mathrm{cm}^3$. The integrated value of the $\mathrm{Re}\,\mathscr{P}(\mathrm{j}k)$ from measurement gives $5.53\,\mathrm{cm}^3$ which is less than the optimal solution, and as discussed in Example A, the system noise causes negative parts in the measured signal which in turn decreases the integral value. Using the parallel plate capacitor, the polarizability is determined to $\gamma_e = 7.03\,\mathrm{cm}^3$. The sum of the polarizabilities of two objects in Example A is $3.53 + 3.65 = 7.18\,\mathrm{cm}^3$ which is similar to the polarizability of this example. This verifies the additive property of the polarizability in the static limit.

6.3 Double Resonance Structure

In Fig. 6a, the forward scattering of a double resonant structure, consisting of the cylindrical SRR in Example A and an in-house fabricated SRR structure supported by a cuboid-shaped plastic, is shown as solid curves. The in-house fabricated structure is composed of 6×4, 1 mm thick split ring resonators that each has an outer diameter of 4.8 mm and an inner diameter of 4 mm with an air gap of 1×1 mm. As can be seen, the first resonance at $f = 5.5$ GHz is caused by the cylindrical SRR structure and the second resonance at $f = 9$ GHz represents the in-house fabricated object. The convex optimization solution is shown as dashed curves. The second resonance in Fig. 6a has a wider resonance behavior which is mainly due to the dielectric scattering contributions of the plastic support.

The optimal solution from the convex optimization estimates the polarizability to $\mathscr{P}(\mathrm{j}k)/\mathrm{j}k = 6.42\,\mathrm{cm}^3$ as $k \to 0$, and the integration on left hand side in (3.3) over the frequency range $f = [0 - 20]$ GHz is estimated to $5.28\,\mathrm{cm}^3$ which is 88% of the low-frequency approximation. The integration of σ_{tot} from $f = 2$ GHz to $f = 20$ GHz from measurement is $5.4\,\mathrm{cm}^3$. The electric polarizability, γ_e, found from the parallel plate capacitor, is $7.58\,\mathrm{cm}^3$.

The results from this example illustrate that regardless of the shape of the scatterer and its resonance behavior, the total cross section is always bounded by the static polarizability. In this particular example, the structure can be designed to have more resonances or wider bandwidth. However, in either case the total interaction between the fields and the object are bounded by the static polarizability that is measured in the parallel plate capacitor.

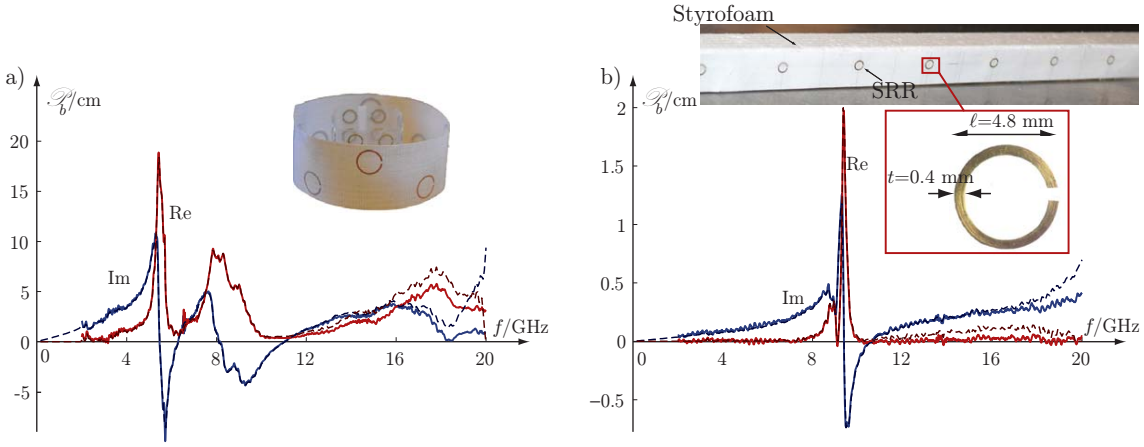

Figure 6: a) Measured values (solid curves) and the optimal solution (dashed curves) for the forward scattering of a in-house fabricated cuboid-shaped SRR structure inside a cylinder of split ring resonator with the diameter of unit element, $\ell = 4.8\,\text{mm}$ for the inner object and $\ell = 8\,\text{mm}$ for the outer one. b) Measured values (solid curves) and the optimal solution (dashed curves) for the forward scattering of a in-house fabricated planar periodic structure of split ring resonators with 20 mm spacing between each two elements.

6.4 Planar periodic structure

In order to show the optical theorem for periodic structures discussed in 2.1, we consider a planar periodic structure consisting of split ring resonators attached to a Styrofoam slab as shown in Fig. 6b. The forward scattering of the periodic structure using (2.4) is shown in Fig. 6b. Solid lines show the measured values and the dashed lines are the optimal solution from the convex optimization problem. Choosing an appropriate upper bound on the polarizability, *i.e.*, $\gamma_\text{u} = 0.211\,\text{cm}^3$, in (4.9) the static polarizability per unit cell is estimated to $\mathscr{P}(\text{j}k)/\text{j}k = 0.208\,\text{cm}^3$ as $k \to 0$. The left hand side of the sum rule by integrating σ_tot/k^2 is estimated to $0.158\,\text{cm}^3$ and $0.111\,\text{cm}^3$ for the optimal solution and the measured values, respectively. Using the parallel plate capacitor, the static polarizability is measured over 11, 4 and 2 unit cells separately. All the measured values provide similar results for a unit cell, *i.e.*, $\gamma_\text{e} = 0.196 \pm 0.001\,\text{cm}^3$.

7 Conclusions

In this paper, a sum rule for parallel plate waveguides is investigated. We have demonstrated that the total interaction between the electromagnetic field and a scatterer, integrated over all frequencies, is bounded by the static polarizability of the object. We show that the optical theorem inside the waveguide is solely related to the zeroth order propagating mode and therefore the problem can be treated as a 2D scattering problem. A parallel plate waveguide has been used to determine the

total cross section and a parallel plate capacitor to find the static polarizability of various resonant scattering objects. The accuracy of the measurements is improved by applying a convex optimization problem to identify the passive system. The left hand side of the sum rule from dynamic measurements is on the average about 80% of the polarizability in the right hand side measured in the parallel plate capacitor.

Acknowledgment

This work was supported in part by Swedish Research Council (VR) and the Swedish Foundation of Strategic Research (SSF).

Appendix A Cylindrical wave mode expansion

The scattered fields inside the parallel plate waveguide are decomposed to TE and TM modes:

$$\text{TE modes}: \begin{cases} \boldsymbol{E}_{\rm s} = E_\rho \hat{\boldsymbol{\rho}} + E_\phi \hat{\boldsymbol{\phi}} \\ \boldsymbol{H}_{\rm s} = H_\rho \hat{\boldsymbol{\rho}} + H_\phi \hat{\boldsymbol{\phi}} + H_z \hat{\boldsymbol{z}} \end{cases}$$

$$\text{TM modes}: \begin{cases} \boldsymbol{E}_{\rm s} = E_\rho \hat{\boldsymbol{\rho}} + E_\phi \hat{\boldsymbol{\phi}} + E_z \hat{\boldsymbol{z}} \\ \boldsymbol{H}_{\rm s} = H_\rho \hat{\boldsymbol{\rho}} + H_\phi \hat{\boldsymbol{\phi}} \end{cases}$$

According to (2.6) and Fig. 1c , $\hat{\boldsymbol{n}} = \hat{\boldsymbol{\rho}}$, $\hat{\boldsymbol{z}} \cdot \boldsymbol{E}_{\rm s} = E_{\rm z}^{\rm TM}$ and $\boldsymbol{H}_{\rm s} \times \hat{\boldsymbol{n}} = -H_\phi \hat{\boldsymbol{z}}$ for both TE and TM modes. This reduces (2.6) to

$$P_{\rm tot} = \frac{-1}{2\eta_0} \,\mathrm{Re}\left\{ E_0^* \sum_{m=0}^{\infty} \sum_{n=0}^{\infty} \int_0^b \int_0^{2\pi} \mathrm{e}^{\mathrm{j}kx} \big(E_{\rm z}^{\rm TM} \cos\phi - \eta_0 (H_\phi^{\rm TE} + H_\phi^{\rm TM}) \big) \rho \,\mathrm{d}\phi \,\mathrm{d}z \right\}, \quad \text{(A.1)}$$

where the integral is on a circular cylindrical surface defined by $\sqrt{x^2+y^2} = \rho =$ constant. The expansion of the fields in cylindrical waves for the mn mode is given by [2]

$$E_{\rm z,mn}^{\rm TM}(\rho,\phi,z) = -\mathrm{j} B_{mn} \frac{k_\rho^2}{\omega\mu\epsilon} H_m^{(2)}(k_\rho \rho) \cos(m\phi) \cos(\frac{n\pi}{b} z) \quad \text{(A.2)}$$

$$H_{\phi,\rm mn}^{\rm TM}(\rho,\phi,z) = -B_{mn} \frac{k_\rho}{\mu} H_m^{(2)\prime}(k_\rho \rho) \cos(m\phi) \cos(\frac{n\pi}{b} z) \quad \text{(A.3)}$$

$$H_{\phi,\rm mn}^{\rm TE}(\rho,\phi,z) = \mathrm{j} A_{mn} \frac{mn\pi}{\omega\mu\epsilon\rho h} H_m^{(2)}(k_\rho \rho) \sin(m\phi) \cos(\frac{n\pi}{b} z), \quad \text{(A.4)}$$

where $m = (0, 1, ...)$ is the index for the cylindrical wave and n for the waveguide modes, A_{mn} and B_{mn} are the frequency dependent expansion coefficients for TE (n=1,2,...) and TM (n=0,1,...) modes, respectively and $k_\rho = \sqrt{k^2 - (\frac{n\pi}{b})}$ is the

wavenumber in the ρ direction. Vertical variations are solely based on $\cos(\frac{n\pi}{b}z)$ and by integrating the variations over the z-axis we get

$$c_n = \int_0^b \cos(\frac{n\pi}{b}z)\,\mathrm{d}z = \begin{cases} b & \text{for } n = 0 \\ 0 & \text{for } n > 0. \end{cases} \tag{A.5}$$

It should be pointed out that all higher modes have zero contribution and only the zeroth order mode remains and thus, $k_\rho = k$. The $\phi-$dependence in (A.1) is in the exponential coefficient and also in $\cos(m\phi)$ which is hidden in the fields. By using $x = \rho\cos(\phi)$ and using the integral representation of the Bessel function we get [13, p. 140]

$$\int_0^{2\pi} \mathrm{e}^{\mathrm{j}k\rho\cos\phi}\cos(m\phi)\,\mathrm{d}\phi = 2\pi\mathrm{j}^m J_m(k\rho), \tag{A.6}$$

where $J_m(k\rho)$ is the Bessel function of the first kind and order m. Using (A.5) and (A.6) and the fact that only the zeroth order mode contributes in the optical theorem, the total power in (A.1) is simplified to

$$P_{\text{tot}} = \frac{\rho}{2\eta_0}\,\mathrm{Re}\left\{E_0^* \sum_{m=0}^{\infty} 2\pi\mathrm{j}^m k c_0 B_{m0} b[H_m^{(2)}(k\rho)J_m'(k\rho) - H_m^{(2)\prime}(k\rho)J_m(k\rho)]\right\}, \tag{A.7}$$

where c_0 is the speed of light in vacuum. The statement inside the bracket is similar to Wronskian of the Bessel functions. By expanding the Hankel functions to Bessel and Neumann functions and using the Wronskian [1], *i.e.*, $[H_m^{(2)}J_m'(k\rho) - H_m^{(2)\prime}(k\rho)J_m(k\rho)] = \frac{2}{\pi k\rho}$ the total power can be simplified to

$$P_{\text{tot}} = \frac{1}{2\eta_0}\sum_{m=0}^{\infty}\mathrm{Re}\left\{\frac{4}{k}E_0^*\mathrm{j}^{m+1}kc_0bB_{m0}\right\}. \tag{A.8}$$

This is valid for any ρ and by normalizing the total power with the incident power flux, $|E_0|^2/2\eta_0$, the total cross section can be written as

$$\sigma_{\text{tot}} = -4b\,\mathrm{Re}\left\{\frac{E_0^* f_{\text{s}}(k)}{\mathrm{j}k|E_0|^2}\right\}, \tag{A.9}$$

where we used the definition in (2.8).

Appendix B Transmission in the waveguide

The TEM horn antenna inside the waveguide is used for smooth transition from the antenna port to the waveguide. The reflection coefficient, $|S_{11}|$ in Fig. 7 shows that the antenna has the best performance up to 12 GHz. Since the signal to noise ratio inside the waveguide is not a major issue, the matching of -5 dB at higher frequencies is also acceptable. The transmission inside the waveguide $|S_{21}|$ is shown in Fig. 7

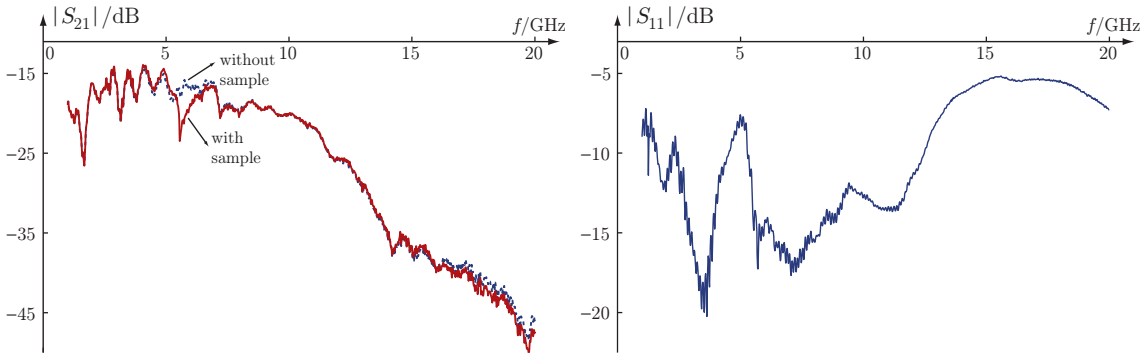

Figure 7: Measured values of $|S_{21}|$ in the presence (solid) and the absence (dashed) of the object is shown in the figure on the left. The figure on the right side shows the $|S_{11}|$ in the absence of the object.

for the first example in the presence and the absence of the object. The transmission is maximum for the lower frequencies since the antenna is better matched and the gain is higher. The other effect that declines the performance is the existence of the higher order modes for higher frequencies. It is obvious from the figure that the transmission is clearly different in the absence and the presence of the object, even for higher frequencies where the scattering is very low and the antenna performance is not as good as the lower frequencies.

References

[1] M. Abramowitz and I. A. Stegun, editors. *Handbook of Mathematical Functions*. Applied Mathematics Series No. 55. National Bureau of Standards, Washington D.C., 1970.

[2] C. A. Balanis. *Advanced Engineering Electromagnetics*. John Wiley & Sons, New York, 1989.

[3] A. Bernland, A. Luger, and M. Gustafsson. Sum rules and constraints on passive systems. *J. Phys. A: Math. Theor.*, **44**(14), 145205, 2011.

[4] S. P. Boyd and L. Vandenberghe. *Convex optimization*. Cambridge Univ Pr, 2004.

[5] F. Capolino, editor. *Theory and Phenomena of Metamaterials*. CRC Press, 2009.

[6] M. Gustafsson. Time-domain approach to the forward scattering sum rule. *Proc. R. Soc. A*, **466**, 3579–3592, 2010.

[7] M. Gustafsson, M. Cismasu, and S. Nordebo. Absorption efficiency and physical bounds on antennas. *International Journal of Antennas and Propagation*, **2010**(Article ID 946746), 1–7, 2010.

[8] M. Gustafsson, C. Sohl, and G. Kristensson. Physical limitations on antennas of arbitrary shape. *Proc. R. Soc. A*, **463**, 2589–2607, 2007.

[9] M. Gustafsson, C. Sohl, and G. Kristensson. Illustrations of new physical bounds on linearly polarized antennas. *IEEE Trans. Antennas Propagat.*, **57**(5), 1319–1327, May 2009.

[10] M. Gustafsson. Sum rule for the transmission cross section of apertures in thin opaque screens. *Opt. Lett.*, **34**(13), 2003–2005, 2009.

[11] M. Gustafsson and D. Sjöberg. Physical bounds and sum rules for high-impedance surfaces. *IEEE Trans. Antennas Propagat.*, **59**(6), 2196–2204, 2011.

[12] M. Gustafsson, I. Vakili, S. E. B. Keskin, D. Sjöberg, and C. Larsson. Optical theorem and forward scattering sum rule for periodic structures. *IEEE Trans. Antennas Propagat.*, **60**(8), 3818–3826, 2012.

[13] J. D. Jackson. *Classical Electrodynamics.* John Wiley & Sons, New York, third edition, 1999.

[14] I. S. Kac and M. G. Kreĭn. R-functions — analytic functions mapping the upper halfplane into itself. *Amer. Math. Soc. Transl.(2)*, **103**, 1–18, 1974.

[15] S. M. Kay. *Fundamentals of Statistical Signal Processing, Estimation Theory.* Prentice-Hall, Inc., NJ, 1993.

[16] G. Kristensson. The polarizability and the capacitance change of a bounded object in a parallel plate capacitor. *Physica Scripta*, **86**(3), 035405, 2012.

[17] N. Marcuvitz. *Waveguide Handbook.* McGraw-Hill, New York, 1951.

[18] B. Munk. *Frequency Selective Surfaces: Theory and Design.* John Wiley & Sons, New York, 2000.

[19] R. Newton. Optical theorem and beyond. *Am. J. Phys*, **44**, 639–642, 1976.

[20] H. M. Nussenzveig. *Causality and dispersion relations.* Academic Press, London, 1972.

[21] E. M. Purcell. On the absorption and emission of light by interstellar grains. *J. Astrophys.*, **158**, 433–440, 1969.

[22] D. Sjöberg. Low frequency scattering by passive periodic structures for oblique incidence: low pass case. *J. Phys. A: Math. Theor.*, **42**, 385402, 2009.

[23] D. R. Smith, S. Schultz, P. Markos, and C. M. Soukoulis. Determination of effective permittivity and permeability of metamaterials from reflection and transmission coefficients. *Phys. Rev. B*, **65**, 195104–195108, 2002.

[24] C. Sohl and M. Gustafsson. A priori estimates on the partial realized gain of Ultra-Wideband (UWB) antennas. *Quart. J. Mech. Appl. Math.*, **61**(3), 415–430, 2008.

[25] C. Sohl, M. Gustafsson, and G. Kristensson. Physical limitations on broadband scattering by heterogeneous obstacles. *J. Phys. A: Math. Theor.*, **40**, 11165–11182, 2007.

[26] C. Sohl, C. Larsson, M. Gustafsson, and G. Kristensson. A scattering and absorption identity for metamaterials: experimental results and comparison with theory. *J. Appl. Phys.*, **103**(5), 054906, 2008.

[27] J. W. Strutt. On the light from the sky, its polarization and colour. *Phil. Mag.*, **41**, 107–120 and 274–279, April 1871. Also published in Lord Rayleigh, Scientific Papers, volume I, Cambridge University Press, Cambridge, 1899.

[28] J. van Bladel. *Electromagnetic Fields*. Hemisphere Publication Corporation, New York, 1986. Revised Printing.

[29] F. Yang and Y. Rahmat-Samii. *Electromagnetic band gap structures in antenna engineering*. Cambridge University Press, 2009.